Frequency Domain Modelling for Assessment of Hilbert and SOGI Based Single-Phase Synchronisation

Sjur Føyen*, Chen Zhang†, Olav Fosso* and Marta Molinas†
*Dept. of Electric Power Engineering, Norwegian University of Science and Technology
Trondheim, Norway
†Dept. of Engineering Cybernetics, Norwegian University of Science and Technology
Trondheim, Norway
Email: foyen.sjur@ntnu.no

Abstract—Two different single-phase synchronisation schemes based on orthogonal system generation (OSG) are modelled in the linear, time-periodic framework. The frequency adaptive Hilbert phase locked loop (PLL) and the frequency-fixed second-order-generalised-integrator (SOGI) PLL fit smoothly into existing models for the synchronous reference frame PLL, due to the linear and decoupled nature of the orthogonal system generation. The harmonic transfer functions are established, and shown to accurately capture the frequency coupling properties of the synchronisation techniques. This modelling approach is a milestone towards the ultimate goal of assessing the impact of synchronisation on single-phase converter small-signal stability. The analytic models are compared to simulations, through use of a chirp input signal instead of the typical frequency sweeping technique. The conceptual differences between the Hilbert PLL and SOGI PLL are highlighted, yet without attempts at asserting superiority of either scheme.

Index Terms—Synchronisation, PLL, Hilbert, SOGI, harmonic transfer function, single-phase systems

I. INTRODUCTION

Orthogonal system generator (OSG) based phase detector (PD) is a prevalent class of single-phase grid synchronisation techniques [1], dedicated to real-time phase estimation of a sinusoidal signal. The majority of power converters contain control loops that depend on the grid voltage angle, and accurate modelling of the phase estimation plays a vital role in assessing the stability of the converter circuit. The impact of the OSG is often ignored, justified by the fast response of the OSG compared to the PD - when the PD is achieved through a phase locked loop (PLL). Although this is sufficient for describing its transient response, a detailed model is necessary to enable our understanding of single-phase synchronisation techniques in the frequency domain. In essence, two concerns need additional consideration: quadrature signal generation filter effects and change of reference frame. The latter is the root cause of the frequency coupling phenomenon in the synchronisation techniques and together they make the SISO linear time-invariant model an insufficient tool for frequency domain modelling [2].

A better approach is to apply linear, time-periodic (LTP) theory and use harmonic transfer functions (HTFs) [2], which can capture the dynamics caused by the change in reference frame and gain inequality between the in-phase and quadrature voltage transfer functions. Higher appreciation of the HTF approach can be found by contemplating the impedance modelling of converter systems, see [3] [4] for examples of three-phase VSC analysis. Impedance analyses of single-phase converters including the OSG-PD can be found in [5] and [6], which derive analytic models for the frequency-fixed second order generalised integrator (SOGI) PLL based on harmonic linearisation.

In power electronics based single-phase converters, several control layers require accurate phase estimation for their intended purpose. In Figure 1, a simple voltage source converter is depicted with a proportional-resonant current controller, where the phase is needed to convert the dq current reference to the stationary reference frame. The input/output relation of the synchronisation scheme, i.e. from u_a to θ, must be determined
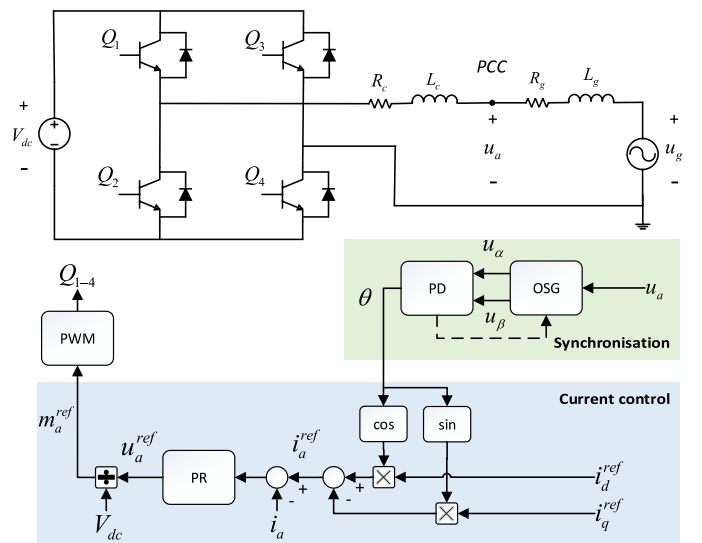

Figure 1. Single-phase VSC with OSG-PD synchronisation and proportional-resonant current control

to include its dynamics in a stability evaluation.

Two types of OSG based single-phase synchronisation schemes are considered in this article. Hilbert transformers are often the go-to for applications in need of orthogonal signal generation. This paper will consider the finite impulse response (FIR) realisation of the Hilbert transform, although the infinite impulse response (IIR) version may prove to be a promising candidate as well [7]. Unjustly disregarded in literature due to their complexity, FIR Hilbert transformers (from here on the FIR prefix is omitted) offer an inherent robustness to frequency changes which eliminates the need for a frequency feedback to the OSG. This, combined with a completely linear process of orthogonal system generation, enables a straightforward model in the frequency domain. A practical introduction to the design and implementation of a Hilbert OSG-PD can be found in [8].

The Hilbert PLL is compared with the standard SOGI-PLL without frequency feedback to the OSG, as originally designed in [9]. The latter does not adapt to frequency changes in the input voltage, which may be impractical for some applications. The frequency adaptive version, along with other intricate single-phase synchronisation techniques, are the real competitors of the Hilbert-PLL; all frequency adaptive OSG-PD's sacrifice performance for robustness. Since most of the advanced OSG-PLLs have a feedback from the PLL to the OSG, or have extra nonlinear feedback paths, they pose a considerable greater challenge to model in the same framework. However, recent efforts towards removing the OSG-PD feedback have been made for different synchronisation schemes. In [10], the frequency feedback of the SOGI-PLL could have been completely removed had it not been for the amplitude compensation in the quadrature signal. In [11], the decoupling is achieved for the transport-delay based PLL. The SOGI frequency locked loop (FLL) also shares the decoupling trait, and some attempts at modelling the SOGI FLL in the LTP framework have been conducted in [12] and [13], although with different objectives than frequency domain modelling. Continued efforts in this direction can hopefully lead to comparable competitors for the Hilbert PLL.

II. HILBERT AND SOGI PLL

The concept of an OSG-PD is to generate a 90-degree shifted version of a sinusoidal signal, and determine the phase as the angle of the rotating vector in the complex plane. Several methods that adopt this approach are outlined in [1], with phase detection realised through a PLL. Figure 2 and Figure 3 show the structure of the frequency adaptive SOGI-PLL and the Hilbert-PLL. One of the striking differences between the two is the independent orthogonal system generator in the Hilbert-PLL. The SOGI-OSG is described in the Laplace domain by the transfer functions

$$h_\alpha(s) = \frac{u_\alpha(s)}{u_a(s)} = \frac{k\omega_f s}{s^2 + k\omega_f s + \omega_f^2} \tag{1}$$

$$h_\beta(s) = \frac{u_\beta(s)}{u_a(s)} = \frac{k\omega_f^2}{s^2 + k\omega_f s + \omega_f^2} \tag{2}$$
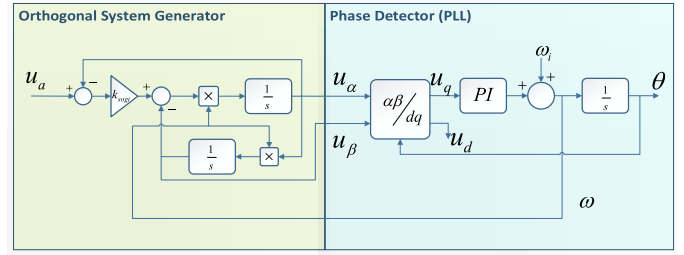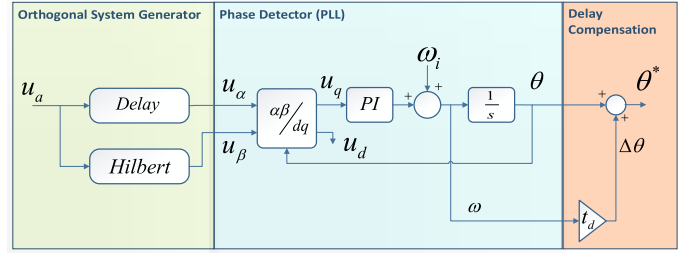

Figure 2. SOGI-PLL with frequency feedback

Figure 3. Hilbert-PLL with delay compensation

where k is the SOGI gain, ω_f is the resonance (fundamental) frequency and u_a is the input voltage. As mentioned, the basic SOGI-PLL with fixed resonance frequency is adopted in this paper. This is equivalent to replacing the feedback in Fig 2 with a constant term - resulting in a linear and decoupled OSG. Still, it is worth noting that h_α is a bandpass filter, while h_β provides lowpass filter capabilities. Although the two signals are orthogonal to one another in the whole frequency range, the gain mismatch results in frequency couplings and subsequently increased complexity in the modelling and analysis stage.

The Hilbert OSG has no dependency of the frequency in the care-band, i.e. the assumed frequency range of the grid fundamental harmonic. Yet this does not come without drawbacks. The Hilbert-PLL (Figure 3) in its most general form has: little to no filtering capabilities in the stationary $\alpha\beta$ reference frame; a constant time delay in the range of 5-10ms (depending on the filter design); and, compensation for the steady-state error as the PLL locks to a time-delayed signal. The compensation term θ_{delay} is the angle difference caused by the time delay - at the fundamental frequency w. To qualitatively determine the value of this trade in terms of stability seems a daunting task, as the final performance is determined by the complete system - included PLL, converter and grid dynamics. Another aspect with the FIR filter is that it is designed for a specific sampling rate. Although two filters designed for different rates have similar frequency responses, the computational effort increases with the rate and demands attention at higher than $20\,\mathrm{kHz}$.

A Hilbert filter designed as in [8], has the amplitude response of Figure 4. The phase delay is - according to standard FIR filters - linearly increasing with frequency, yet with an additional 90° in the whole frequency range. The transfer functions for the Hilbert OSG are presented in (3)
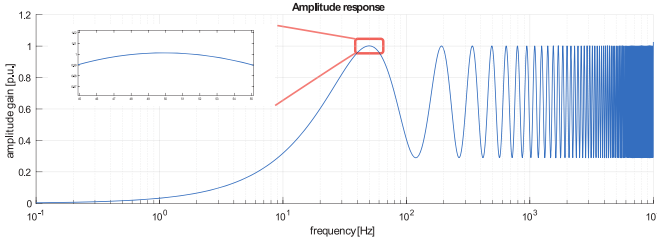
Figure 4. Amplitude response of a FIR Hilbert filter designed as a tradeoff between speed and frequency independence

and (4). Since the FIR filter is digital, the transfer functions are given in the discrete domain as

$$h_\alpha(z) = \frac{u_\alpha(z)}{u_a(z)} = z^{-\frac{L-1}{2}} \tag{3}$$

$$h_\beta(z) = \frac{u_\beta(z)}{u_a(z)} = \sum_{k=1}^{L} h_k \cdot z^{-k} \tag{4}$$

where h_k is the kth filter coefficient in a FIR filter of length L. The Hilbert filter shown in Figure 4 is designed with $L = 265$ for sampling frequency $f_s = 20\,\text{kHz}$, which yields a time delay of $t_{delay} = 6.6\,\text{ms}$ and consequently a phase delay of $\phi_d = 0.66\pi\,\text{rad}$ at $\omega = 2\pi \cdot 50\,\text{rad}\,\text{s}^{-1}$.

III. MODELLING IN THE LINEAR TIME PERIODIC FRAMEWORK

To achieve a model that describes the relation between the input voltage and output phase, the change in reference frame requires additional attention. The following approach is valid for OSG-PLLs based on Parks transformation *without* feedback from the PLL to the OSG. The $\alpha\beta/dq$ transform returns the q-axis voltage

$$u_q = -sin(\theta_{pll})\hat{u}_\alpha + cos(\theta_{pll})\hat{u}_\beta \tag{5}$$

Note that (5)-(7) are given in the time domain. Linearise u_q as a function of the independent variables θ_{pll}, $\hat{u}_\alpha$ and $\hat{u}_\beta$

$$u_q = u_q(\theta_0, \hat{u}_{\alpha 0}, \hat{u}_{\beta 0}) + \nabla u_q(\theta_0, \hat{u}_{\alpha 0}, \hat{u}_{\beta 0}) \cdot (\Delta\theta, \Delta\hat{u}_\alpha, \Delta\hat{u}_\beta) \tag{6}$$

where ∇ denotes the gradient. Rearranging (6) yields

$$\Delta u_q = -U_{d0}\Delta\theta_{pll} - sin(\theta_0)\Delta u_\alpha + cos(\theta_0)\Delta u_\beta \tag{7}$$

where $U_{d0} = cos(\theta_0)\hat{u}_{\alpha 0} + sin(\theta_0)\hat{u}_{\beta 0}$.

Then, (7) must be transformed to the frequency domain

$$\mathbf{\Delta u}_q = -\mathbf{U}_{d0}\mathbf{\Delta\theta}_{pll} - \mathbf{A}_{sin\theta_0}\mathbf{\Delta u}_\alpha + \mathbf{A}_{cos\theta_0}\mathbf{\Delta u}_\beta \tag{8}$$

$\mathbf{U}_{d0}$, $\mathbf{A}_{sin\theta_0}$ and $\mathbf{A}_{cos\theta_0}$ are Toeplitz matrices of $U_{d0}(t)$, $cos(\theta_0)$ and $sin(\theta_0)$. The Toeplitz matrix is generally represented by a matrix A on the form

$$\mathbf{A} = \begin{bmatrix} \ddots & \ddots & \ddots & \ddots & \ddots \\ \ddots & A_0 & A_{-1} & A_{-2} & \ddots \\ \ddots & A_{+1} & A_0 & A_{-1} & \ddots \\ \ddots & A_{+2} & A_{+1} & A_0 & \ddots \\ \ddots & \ddots & \ddots & \ddots & \ddots \end{bmatrix} \tag{9}$$

where A_k is the kth fourier coefficient of $A(t)$. $\mathbf{A}_{sin\theta_0}$ and $\mathbf{A}_{cos\theta_0}$ become

$$\mathbf{A}_{sin\theta_0} = \begin{bmatrix} \ddots & \ddots & \ddots & \ddots & \ddots \\ \ddots & 0 & -\frac{1}{2i} & 0 & \ddots \\ \ddots & \frac{1}{2i} & 0 & -\frac{1}{2i} & \ddots \\ \ddots & 0 & \frac{1}{2i} & 0 & \ddots \\ \ddots & \ddots & \ddots & \ddots & \ddots \end{bmatrix}, \mathbf{A}_{cos\theta_0} = \begin{bmatrix} \ddots & \ddots & \ddots & \ddots & \ddots \\ \ddots & 0 & \frac{1}{2} & 0 & \ddots \\ \ddots & \frac{1}{2} & 0 & \frac{1}{2} & \ddots \\ \ddots & 0 & \frac{1}{2} & 0 & \ddots \\ \ddots & \ddots & \ddots & \ddots & \ddots \end{bmatrix} \tag{10}$$

For the PLL, the open loop transfer function from Δu_q to $\Delta\theta_{pll}$ consists of a PI-controller with parameters k_p and k_i, and an integrator.

$$G_{pll}(s) = \frac{k_p s + k_i}{s^2} \tag{11}$$

The open loop transfer function $\mathbf{G}_{pll}$ from $\mathbf{\Delta u}_q$ to $\mathbf{\Delta\theta}_{pll}$ is a diagonal matrix where each element is a frequency shifted version of the scalar transfer function G_{pll} in (11).

$$\mathbf{G}_{pll} = \begin{bmatrix} \ddots & & & \\ & G_{pll}(s - j\omega_f) & & \\ & & G_{pll}(s) & \\ & & & G_{pll}(s + j\omega_f) \\ & & & & \ddots \end{bmatrix} \tag{12}$$

Then, the loop is closed by combining (8) and (12). Creating two frequency shifted diagonal matrices $\mathbf{H}_\alpha$ and $\mathbf{H}_\beta$ (similar to $\mathbf{G}_{pll}$, but with h_α and h_β as the scalar transfer functions), yields the final model

$$\mathbf{\Delta\theta}_{pll} = \frac{\mathbf{G}_{pll}}{\mathbf{I} + \mathbf{U}_{d0}\mathbf{G}_{pll}}[\mathbf{A}_{sin\theta_0}\mathbf{H}_\alpha + \mathbf{A}_{cos\theta_0}\mathbf{H}_\beta]\mathbf{\Delta u}_a \tag{13}$$

Evidently, (13) is composed of the harmonic transfer functions for the closed loop PLL and the OSG.

$$\mathbf{\Delta\theta}_{pll} = \mathbf{G}_{pll}^{cl}\mathbf{H}_{osg}\mathbf{\Delta u}_a \tag{14}$$

The Hilbert-PLL model is extended with the delay compensation term, which is no more than a lead compensator block.

$$\mathbf{\Delta\theta}_{pll}^* = \mathbf{G}_{delay}\mathbf{\Delta\theta}_{pll}$$
$$= \mathbf{G}_{delay}\mathbf{G}_{pll}^{cl}\mathbf{H}_{osg}\mathbf{\Delta u}_a \tag{15}$$

	k_p	k_i	k_{sog}	T_f
SOGI-PLL	125	6500	1	-
Hilbert-PLL	125	6500	-	10 ms

where

$$G_{delay}(s) = \frac{1 + (T_f + t_d)s}{1 + T_f s} \quad (16)$$

and $\mathbf{G}_{delay}$ is the frequency shifted diagonal matrix of G_{delay}. Note that due to the high order of the Hilbert FIR filter, it is convenient to transform $\mathbf{G}_{delay}$ and $\mathbf{G}_{pll}^{cl}$ to the discrete domain and not $\mathbf{H}_{osg}$ to the Laplace domain.

The frequency shifted matrices are doubly infinite and must be truncated into finite versions for analysis. Restricting the harmonic order to 2, yields a square 5x5 MIMO transfer function $\mathbf{H}$ from $\boldsymbol{\Delta u}_{in}$ to $\boldsymbol{\Delta \theta}_{pll}$ ($\boldsymbol{\Delta \theta}_{pll}^*$ for Hilbert-PLL).

$$\begin{bmatrix} \Delta\theta_{pll}(s - 2j\omega_f) \\ \Delta\theta_{pll}(s - j\omega_f) \\ \Delta\theta_{pll}(s) \\ \Delta\theta_{pll}(s + j\omega_f) \\ \Delta\theta_{pll}(s + 2j\omega_f) \end{bmatrix} = [\mathbf{H}]_{5x5} \begin{bmatrix} \Delta u_a(s - 2j\omega_f) \\ \Delta u_a(s - j\omega_f) \\ \Delta u_a(s) \\ \Delta u_a(s + j\omega_f) \\ \Delta u_a(s + 2j\omega_f) \end{bmatrix} \quad (17)$$

Assuming that U_{d0} does not contain harmonics, and that the amplitude of the input voltage is unity, $\mathbf{U}_{d0}$ becomes the identity matrix. The diagonal elements of $\mathbf{H}_{osg}$ are always zero, and $\mathbf{G}_{pll}^{cl}$ is diagonal as long as U_{d0} is purely the fundamental harmonic. Thus, the diagonal elements of $\mathbf{H}$ are also zero. Through some matrix algebra, one finds that the only nonzero elements are the upper and lower diagonal elements.

The 3'rd column of $\mathbf{H}$ describes the angle response to a single harmonic perturbation in the input voltage u_a. The parameters of the two OSG-PDs are given in Table I, where k_p and k_i are the PI-controller parameters. Due to the above considerations, the only necessary elements to include are $H_{2,3}$ and $H_{4,3}$. The bode plots of these two transfer functions (in Figure 5 and Figure 6) describe the magnitude and phase response of the frequency shifted input waves.

Before proceeding with the verification, a consideration will be made regarding the assumption of ideal orthogonal rotating vectors. If $h_\beta = jh_\alpha$, the two terms of $\mathbf{H}_{osg}$ will add constructively in the upper diagonal, and destructively in the lower. Thus, the upper diagonal of $\mathbf{H}_{osg}$ will be the frequency shifted transfer functions of h_α, while the lower diagonal will be zero. In other words, the assumption leads to a complete neglection of the positive frequency coupling and the impact of h_β on the negative frequency coupling.

IV. VERIFICATION WITH CHIRP INPUT SIGNAL

To verify the HTF model, the frequency response in the low frequency range is investigated. Here, the dynamics due
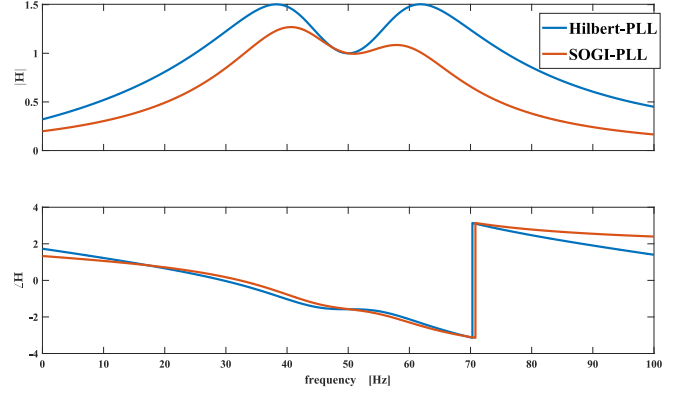

Figure 5. Bode plot for $H_{2,3}$ in the low frequency range
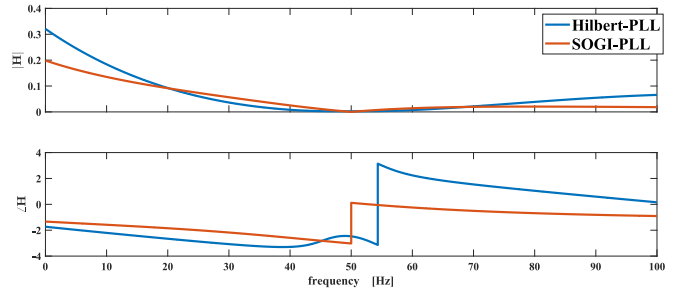

Figure 6. Bode plot for $H_{4,3}$ in the low frequency range

to the OSG and frequency couplings emerge, whereas high frequencies are suppressed by the PLL low-pass characteristics. A chirp perturbation is applied to the input voltage signal, as an alternative method to the established frequency sweeping with single-tone injections. Validation through a chirp signal is not trivial, as steady-state conditions are not guaranteed. A critical question that should be answered in future research is how fast the chirp can be without exceeding a pre-described deviation limit from the steady state assumption. Although this approach certainly deserves a thorough analysis, in this case it is justified by an excellent fit with the analytic model.

A chirp is a constant amplitude sinusoid with linearly increasing frequency. With proportional coefficient ρ and amplitude of 0.01, the perturbation is given as

$$\Delta u_a(t) = 0.01 cos(\int_0^t 2\pi\rho\tau d\tau) \quad (18)$$

Setting $\rho = 1$ - i.e. frequency is equal to time - the input voltage becomes

$$u_a = cos(\omega_f t) + 0.01 cos(\pi t^2) \quad (19)$$

The response for the analytic model is the sum of the response for two frequency shifted sinusoids through $H_{2,3}$ and $H_{4,3}$.

$$\begin{bmatrix} \Delta\theta_{pll}(s - j\omega_f) \\ \Delta\theta_{pll}(s + j\omega_f) \end{bmatrix} = \begin{bmatrix} H_{2,3} \\ H_{4,3} \end{bmatrix} \Delta u_a(s) \quad (20)$$
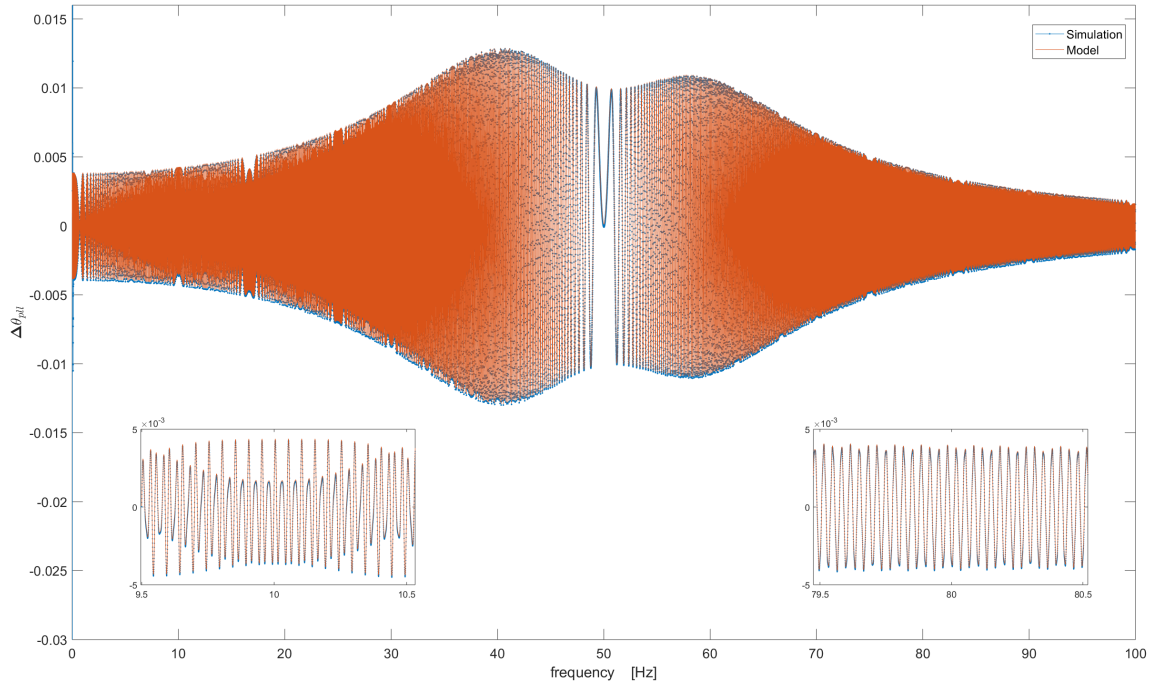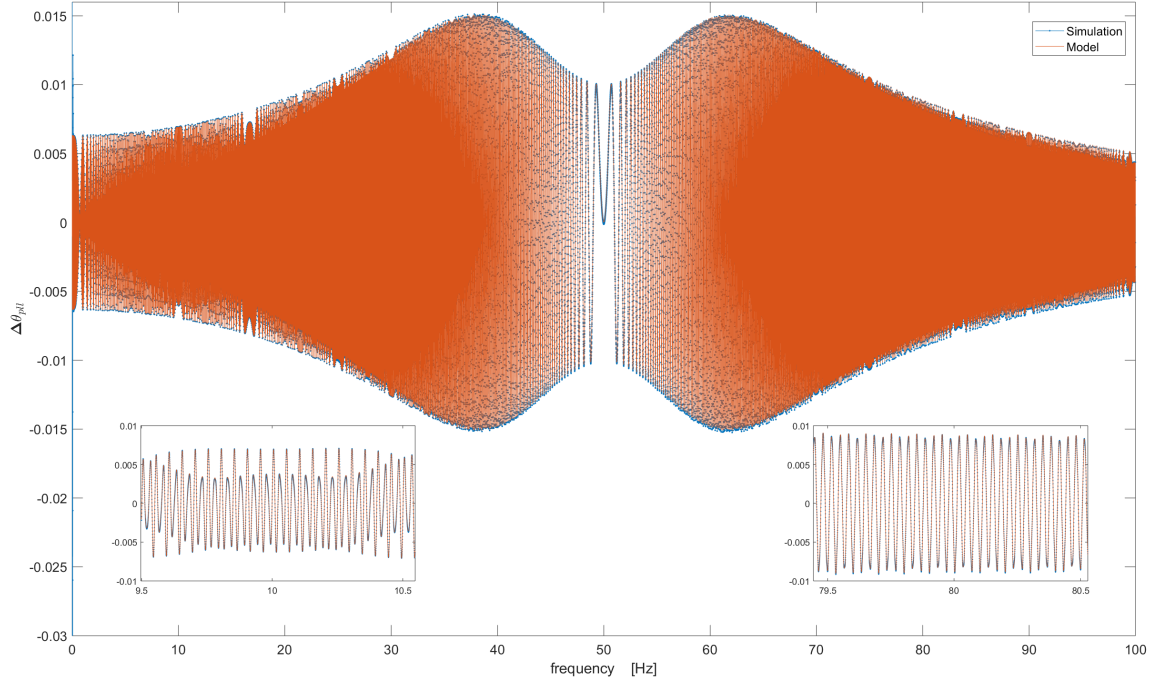
Figure 7. SOGI-PLL chirp

Figure 8. Hilbert-PLL chirp

In the time domain, the response is given by

$$\Delta\theta_{pll}(t) = 0.01\Big(|H_{2,3}(j2\pi t)|cos(t(\pi t - \omega_f) + \angle\, H_{2,3}(j2\pi t))$$

$$+ |H_{4,3}(j2\pi t)|cos(t(\pi t + \omega_f) + \angle H_{4,3}(j2\pi t))\Big) \quad (21)$$

Time domain simulations are compared to (21) both for the SOGI-PLL and for the Hilbert-PLL in Figure 7 and Figure 8, respectively. Both models fit accurately with the simulated waveforms, which is a convincing argument for the HTF approach as well as for chirp perturbation.

Both figures are dominated by the lip-shaped magnitude response of $\mathbf{H}_{2,3}$, i.e for negative shifted frequencies. For frequencies lower - and to some degree higher - than $50\,\mathrm{Hz}$, the positive shifted frequency component contributes to the response. A small comparison of the two PLL schemes can be conducted for the given setup. The lack of filtering in the Hilbert OSG becomes evident in the bode plots. The differences in phase are quite small, particularly for $H_{2,3}$. Again it is emphasised that this article does not aim to conclude on the superiority of either PLL, but rather to highlight the traits that appear in the HTF model. Since Hilbert-PLL is frequency adaptive, and this implementation of SOGI-PLL is non-adaptive, they may also have different uses and a direct comparison would not be fair. For example, by adding a notch filter before the Hilbert OSG, one might improve the filtering capabilities of the Hilbert PLL significantly, yet additional care must be taken to ensure the frequency independence. As the employed PLL is in its most basic form for OSG techniques, one might also consider to modify this for a desired effect on the frequency response.

V. Concluding remarks and future directions

Two OSG-PLLs, one frequency adaptive and the other frequency dependent, have been accurately modelled in the linear, time-periodic framework. Harmonic transfer functions have been demonstrated to encompass the frequency shifting properties of the change in reference frame, as well as include the OSG filter effects. The structured HTF approach results in a frequency domain description that traditional SISO models can never provide. The harmonic transfer function may in turn be used in full converter models, to enable quantitative evaluation of synchronisation performance in terms of stability.

Only after unveiling the true impact of synchronisation on stability, can we make sound performance evaluation of the different synchronisation schemes. The pursuit for this objective is eased by decoupling the OSG from the PD, which is the main advantage of the Hilbert PLL compared to other advanced single-phase synchronisation schemes. Perhaps some day, the nonlinear synchronisation techniques with OSG-PD feedback may be modelled through linearisation approaches within the harmonic transfer function description.

The sacrifice the Hilbert OSG makes for its frequency independence manifests as higher gain in the low frequency range. Time domain simulation through the use of a chirp input wave demonstrates an impeccable fit with the analytic model.

Harmonic transfer function identification through chirp signals could prove useful for OSG-PD systems, if additional efforts are made to extract the frequency coupled bode diagrams from the time-domain response. Also, it has been shown that the OSG filters affect both the positive and negative frequency couplings, which counters the common modelling assumption of ideal orthogonal signals.

References

[1] S. Golestan, J. M. Guerrero, and J. C. Vasquez. Single-phase plls: A review of recent advances. *IEEE Transactions on Power Electronics*, 32(12):9013–9030, Dec 2017.

[2] P. Vanassche, G. Gielen, and W.M.C. Sansen. *Systematic Modeling and Analysis of Telecom Frontends and their Building Blocks*. The Springer International Series in Engineering and Computer Science. Springer US, 2005.

[3] C. Zhang, M. Molinas, A. Rygg, J. Lyu, and X. Cai. Harmonic transfer function-based impedance modelling of a three-phase vsc for asymmetric ac grids stability analysis. *IEEE Transactions on Power Electronics*, pages 1–1, 2019.

[4] X. Wang, L. Harnefors, and F. Blaabjerg. Unified impedance model of grid-connected voltage-source converters. *IEEE Transactions on Power Electronics*, 33(2):1775–1787, Feb 2018.

[5] Y. Liao, Z. Liu, H. Zhang, and B. Wen. Low-frequency stability analysis of single-phase system withdq-frame impedance approach—part i: Impedance modeling and verification. *IEEE Transactions on Industry Applications*, 54(5):4999–5011, Sep. 2018.

[6] H. Zhang, Z. Liu, S. Wu, and Z. Li. Input impedance modeling and verification of single-phase voltage source converters based on harmonic linearization. *IEEE Transactions on Power Electronics*, pages 1–1, 2018.

[7] P. Hao, W. Zanji, and C. Jianye. A measuring method of the single-phase ac frequency, phase, and reactive power based on the hilbert filtering. *IEEE Transactions on Instrumentation and Measurement*, 56(3):918–923, June 2007.

[8] S. Føyen, C. Zhang, O. Fosso, J.A. Suul, M. Molinas, and T. Isobe. Single-phase synchronisation with hilbert transformers: a frequency independent orthogonal system generator. forthcoming.

[9] M. Ciobotaru, R. Teodorescu, and F. Blaabjerg. A new single-phase pll structure based on second order generalized integrator. In *2006 37th IEEE Power Electronics Specialists Conference*, pages 1–6, June 2006.

[10] F. Xiao, L. Dong, L. Li, and X. Liao. A frequency-fixed sogi-based pll for single-phase grid-connected converters. *IEEE Transactions on Power Electronics*, 32(3):1713–1719, March 2017.

[11] S. Golestan, J. M. Guerrero, A. Vidal, A. G. Yepes, J. Doval-Gandoy, and F. D. Freijedo. Small-signal modeling, stability analysis and design optimization of single-phase delay-based plls. *IEEE Transactions on Power Electronics*, 31(5):3517–3527, May 2016.

[12] S. Golestan, J. M. Guerrero, and J. C. Vasquez. Modeling and stability assessment of single-phase grid synchronization techniques: Linear time-periodic versus linear time-invariant frameworks. *IEEE Transactions on Power Electronics*, 34(1):20–27, Jan 2019.

[13] H. Yi, X. Wang, F. Blaabjerg, and F. Zhuo. Impedance analysis of sogi-fll-based grid synchronization. *IEEE Transactions on Power Electronics*, 32(10):7409–7413, Oct 2017.